Supplementary Information (SI) for Energy & Environmental Science.

Supporting Information

Graded desolvation accelerator based on high-entropy alloy with wide-distributed d-band center for high-performance aqueous zinc ion batteries

Yanxin Li, Hongfeng Jia, Lihua Fu, Usman Ali, Liang Zhao, Lingyu Zhang, Lu Li, Yuebo Yang, Chungang Wang, and Bingqiu Liu*,*

Y. Li, H. Jia, L. Fu, U. Ali, Prof. L. Zhao, Prof. L. Zhang, Prof. L Li*, Y. Yang, Prof. C. Wang, Prof. B. Liu*,

EXPERIMENTAL PROCEDURES

Materials:

Bismuth trichloride ($BiCl_3$, 99.99%), antimony trichloride ($SbCl_3$, 99.99%), stannous chloride ($SnCl_2$, 99.99%), indium (III) chloride ($InCl_3$, 99.99%), lead acetate ($(CH_3COO)_2Pb$, 99.9%), and dimethylformamide (DMF) were obtained from Energy Chemical. Zinc sulfate and Zn foils (purity 99.99%) were purchased from Sigma-Aldrich. All reagents were used directly without further purification. Deionized (DI) water was thoroughly used during the experiment.

Preparation of HEA-CFP:

0.25 mmol $BiCl_3$ (78.8 mg), $SbCl_3$ (57.0 mg), $SnCl_2$ (47.4 mg), $InCl_3$ (55.3 mg), and $(CH_3COO)_2Pb$ (81.3 mg) were completely dissolved in 2 mL DMF. The solution was adjusted with concentrated hydrochloric acid until it was clarified and transparent. The clean filter paper was washed with ethanol and dried in an oven at 50 ^{o}C. After drying, the filter paper was immersed in the above solution for 5 min, and the filter paper was taken out and dried naturally for 12 h. Subsequently, the filter paper was subjected to a constant temperature in an argon-hydrogen gas mixture at 900 ^{o}C for 2 hours to obtain HEA-CFP.

Preparation of $NH_4V_4O_{10}$:

Firstly, 5 mmol NH_4VO_3 was dissolved in 30 ml of deionized water. After stirring at room temperature for 30 min, 2 mmol oxalic acid was added with vigorous stirring for 40 min. The mixture was poured into a 50 ml reactor and reacted at 180 °C for 6 h. After centrifuging and drying, the dark green $NH_4V_4O_{10}$ powder was obtained.

Battery Assembly:

HEA-CFP was utilized as a modified layer for the zinc anode, and assembled between the separator and the zinc anode. The cathode was coated with a mixture of $NH_4V_4O_{10}$, acetylene black, and polyvinylidene fluoride (PVDF) binder (mass ratio 7:2:1) mixed well in NMP solvent onto a stainless steel mesh. NMP was dried in a vacuum oven at 80 °C for 12 h to allow complete volatilization. For Zn/$NH_4V_4O_{10}$ cells, the active material loading of the individual electrode was about 1.8-2.0 mg cm^{-2}. 120 μL aqueous solution of 2 M $ZnSO_4$ was selected as an electrolyte. For Zn/Cu and Zn/Zn symmetric cells, the Cu and Zn electrodes were 12 mm in diameter and the electrolyte was 2 M $ZnSO_4$. For the assembly of cells with electrodes containing HEA-CFP, the HEA-CFP is pouched into 14 mm and placed between the glass fiber membrane and zinc foil.

Electrochemical measurements:

The electrochemical impedance spectroscopy (EIS) was collected over the frequency range from 100 kHz to 0.1 Hz by PARSTAT MC 2000 A. Cyclic voltammetry (CV), chronoamperometry (CAs), linear scan voltammetry (LSV), and Tafel plot were tested on the CHI760E electrochemical workstation. CV curves of $Zn/NH_4V_4O_{10}$ cells were performed between 0.30 and 1.70 V at a scan rate of 0.1 mV s^{-1}. LSV curves were conducted by the three-electrodes device at a scan rate of 1 mV s^{-1} in 1 M Na_2SO_4 electrolyte. CAs were collected at an overpotential of -150 mV in coin cells. The galvanostatic cycling performance of Zn/Zn and Zn/Cu was performed in coin cells on a Neware Battery Measurement System (Neware, China). The discharge-charge cycling of $Zn/NH_4V_4O_{10}$ was measured on a battery test instrument (CT2001A, LAND, China) within a voltage range of 0.30-1.70 V.

Materials characterization:

X-ray powder diffraction (XRD) analysis was obtained on a D8 Focus diffractometer (Bruker) with Cu-Ka radiation (λ=0.15405 nm). High-resolution transmission electron microscope (HR-TEM) characterizations were taken by JEOLJEM-2100F transmission electron microscope at 200 kV accelerating voltage. Scanning electron microscopy (SEM) images were measured by an XL30 ESEM-FEG field-emission scanning electron microscope (FEI Co.) with an energy-dispersive X-ray spectrum (EDS). Raman spectrum was recorded at room temperature with a JY HR-800 LabRam confocal Raman microscope in a backscattering configuration, with an excitation wavelength of 488 nm. Atomic force microscope (AFM) was performed on Asylum Research Cypher ES. Inductively-coupled plasma optical emission spectroscopy (ICP-OES) measurements were conducted to examine the chemical composition. X-ray photoelectron spectrum (XPS) was tested on an ECSALAB 250 using non-monochromatized Al-Kα radiation. A contact angle measuring device was used to test the wettability of materials (DSA 100, KRUSS).

Computational details:

The high-entropy alloys (HEA, composed of Sb, Sn, Bi, In, and Pb) were studied by density functional theory (DFT). All calculations were performed via OpenMX 3.9.9,[1,2] which provides a fully relativistic DFT implementation with localized pseudoatomic orbitals[3,4] and norm-conserving pseudopotentials[5]. The exchange-correlation interaction was calculated by the generalized gradient approximation (GGA) method with the Perdew−Burke−Ernzerhof (PBE)[6,7] pure functional. SbSnBiInPb (101) were extracted as model systems. The basis functions were taken as optimized pseudo-atomic orbital functions whose pseudopotential was chosen as the standard item. The long-range van der Waals (vdW) interactions were handled by Grimme's DFT-D3 scheme[8]. The accuracy of the real-space numerical integration was specified by the cutoff energy of 300 Ry; the total energy convergence criterion was 1×10^{-6} eV. The k-mesh for Brillouin zones of 5×5 supercells was specified as 1×1×1 mesh. The vacuum layer was set to 20 Å, avoiding the interaction among mirror images[9,10]. As for the structure optimization, all atoms were allowed to fully relax with the FIRE method until the maximum force on any atom was smaller than 0.05 eV/Å. The Gibbs free energy for the process was calculated as:

$$\Delta G=\Delta E+\Delta E_{ZPE}-T\Delta S \qquad (1)$$

where the values of ΔE, ΔE_{ZPE}, and ΔS denote the changes in the DFT energy, the zero-point energy, and the entropy at 298 K, respectively. The activation barrier of each reaction was obtained from climbing-image nudged elastic band (CI-NEB) calculations. The adsorption energy between HEA and Zn was evaluated as follows,

$$E_{ads}=E(HEA\text{-}Zn)-E(HEA)-E(Zn) \qquad (2)$$

where the terms at the right hand are the energies of Zn adsorption on HEA, HEA, and Zn, respectively. Moreover, the charge density difference was expressed as

$$\Delta\rho=\rho(HEA\text{-}Zn(H_2O)_6)-\rho(HEA)-\rho(Zn(H_2O)_6) \qquad (3)$$

and $\rho(HEA\text{-}Zn(H_2O)_6)$, $\rho(HEA)$, and $\rho(Zn(H_2O)_6)$ are charge densities of $Zn(H_2O)_6$ adsorption on HEA, HEA, and $Zn(H_2O)_6$.

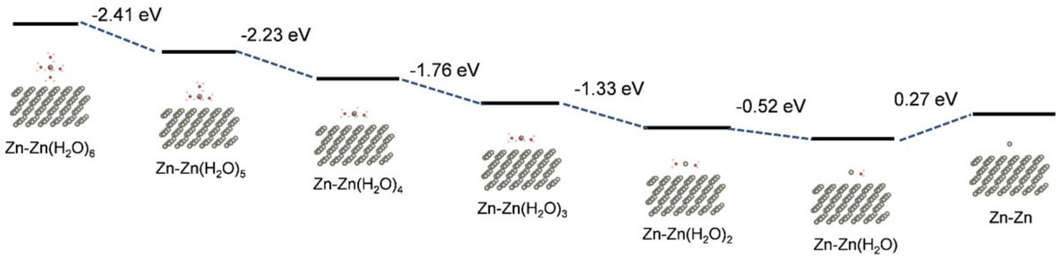

Fig. S1 Energy during the sequential desolvation on bare Zn.

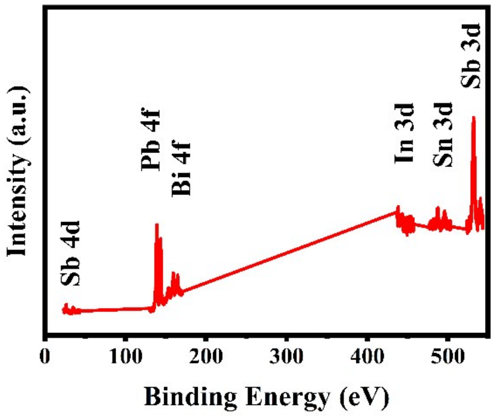

Fig. S2 XPS spectrum of HEA-CFP.

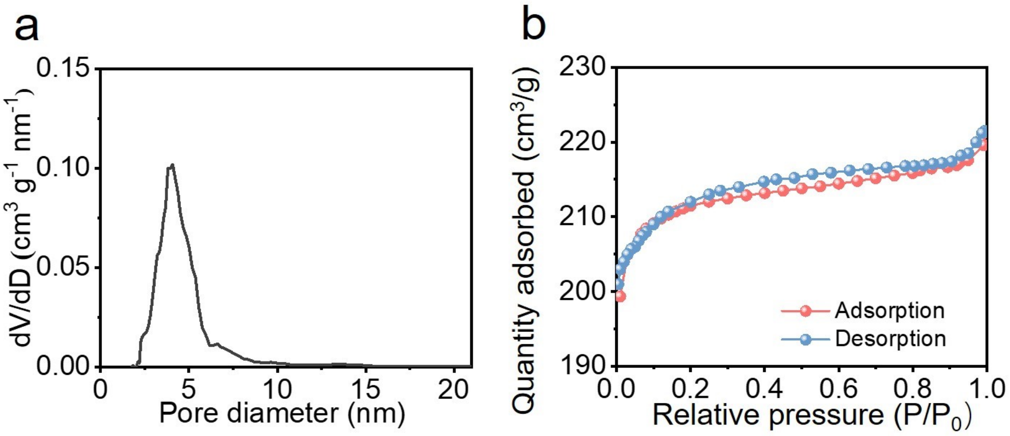

Fig. S3 (a) Pore size distribution and (b) N_2 adsorption-desorption isotherm of HEA-CFP.

Fig. S4 Raman spectrum of HEA-CFP.

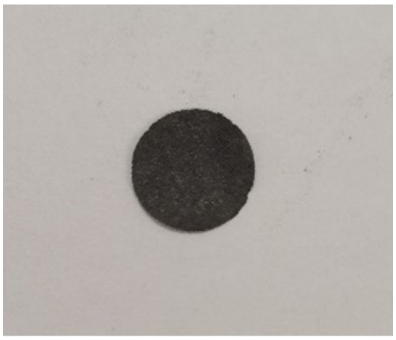

Fig. S5 Optical photograph of HEA-CFP.

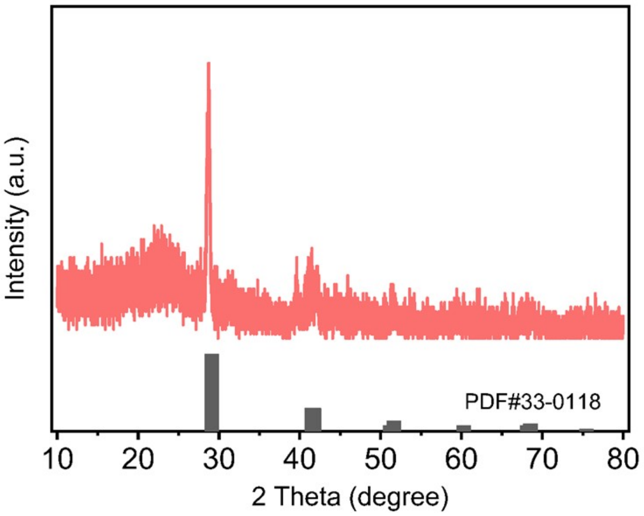

Fig. S6 XRD pattern of HEA-CFP after immersion in the electrolyte for 7 days.

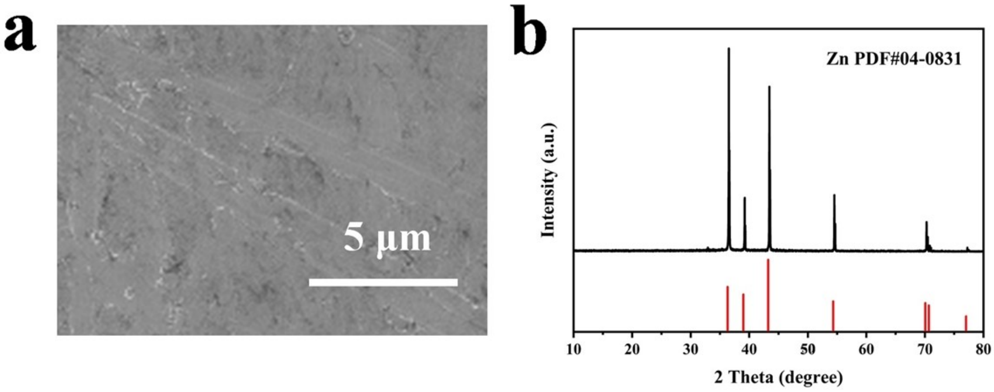

Fig. S7 (a) XRD pattern and (b) SEM image of bare Zn.

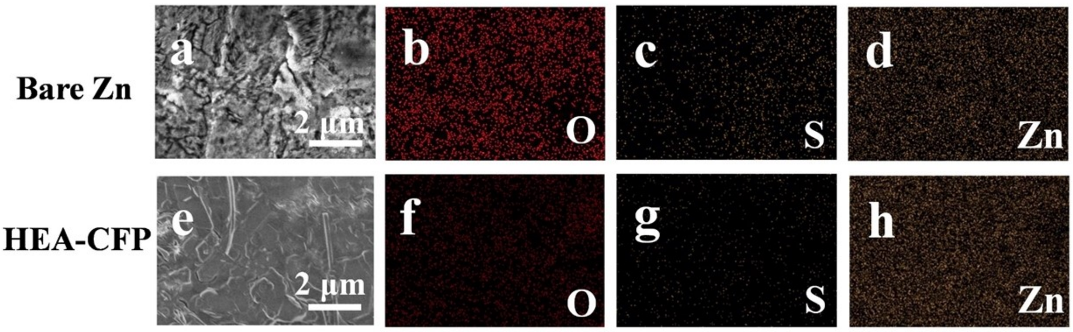

Fig. S8 SEM and mapping results of (a-d) bare Zn and Zn surface in (e-h) HEA-CFP after immersion in the electrolyte for 7 days.

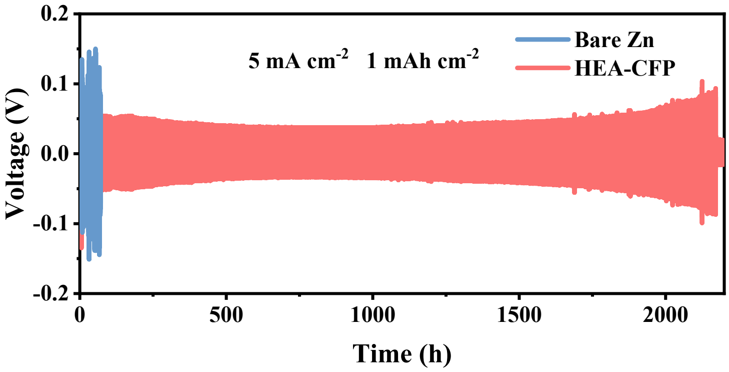

Fig. S9 Cycling performance of the symmetric cells at high current densities (5 mA cm^{-2}).

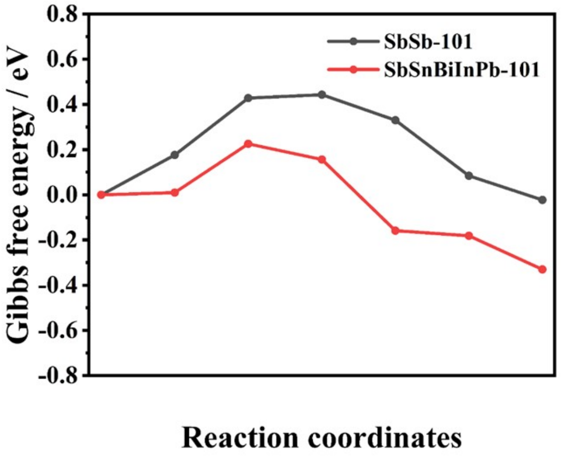

Fig. S10 Diffusion energy barriers for Zn^{2+} migration on SbSn-(101) and SbSnBiInPb-(101).

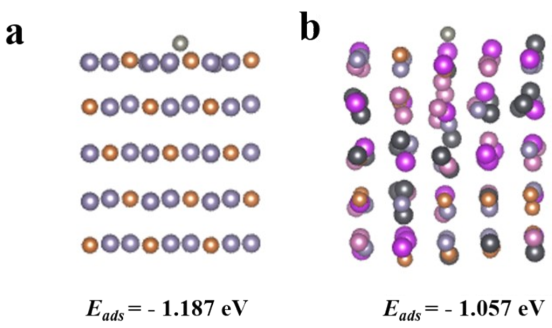

Fig. S11 Adsorption of Zn atoms on the surfaces of (a) SbSn-(101) and (b) SbSnBiInPb-(101).

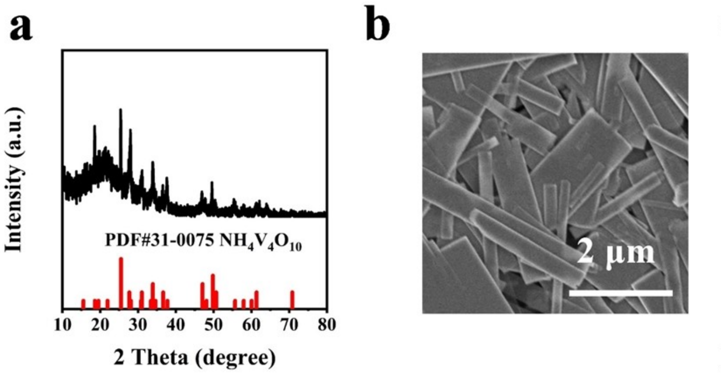

Fig. S12 (a) XRD pattern and (b) SEM image of $NH_4V_4O_{10}$.

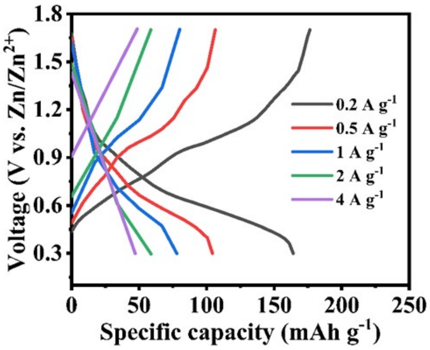

Fig. S13 Charge and discharge curves at different current densities of Bare Zn/$NH_4V_4O_{10}$.

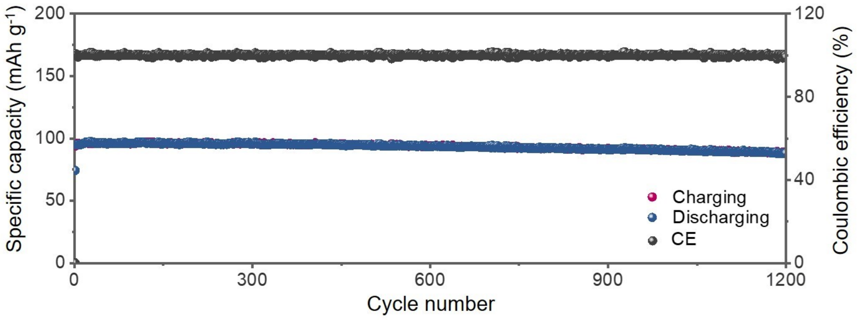

Fig. S14 Cycling performance of full cells with a low N:P ratio (1.5) at 10 A g^{-1}.

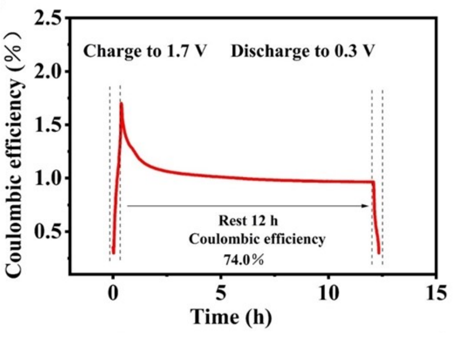

Fig. S15 Self-discharge curve of Bare Zn/$NH_4V_4O_{10}$ cells.

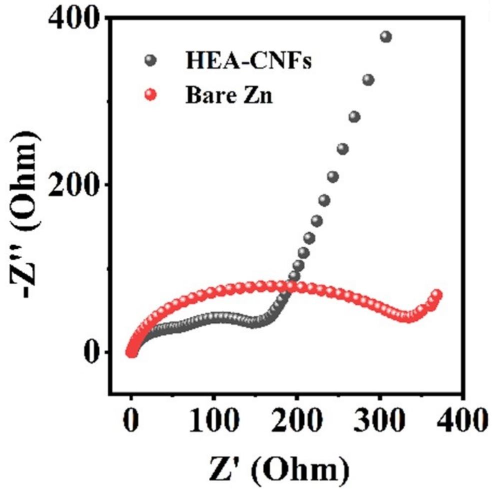

Fig. S16 EIS plots of HEA-CFP and Bare Zn cells.

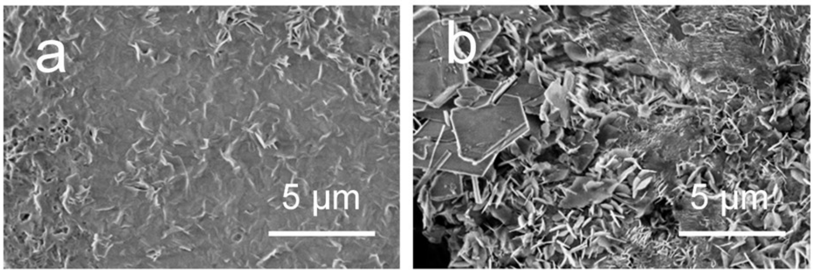

Fig. S17 SEM images of (a) HEA-CFP and (b) bare Zn in pouch cells after cycling.

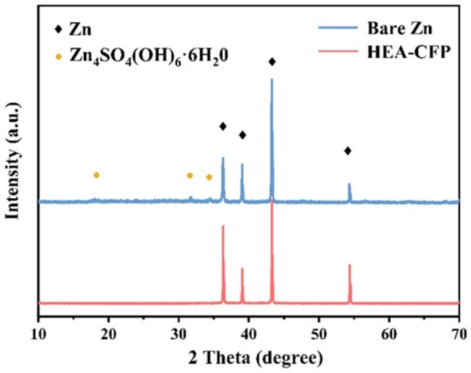

Fig. S18 XRD patterns of the bare Zn and Zn surface of HEA-CFP in Zn/$NH_4V_4O_{10}$ cells after cycling.

Table S1. The refined crystallographic data of HEA and SnSb obtained from XRD

Rietveld refinements.

Sample	**a (=b)/Å**	**c/Å**	**Volume/Å^3**
HEA	4.33	5.32	86.37
SnSb	4.33	5.35	86.63

Table S2. Comparison of main parameters and cycling property for this work with other previous works.

Electrode	**Current density (mA cm^{-2})**	**Areal capacity (mAh cm^{-2})**	**Cycling life (h)**	**Ref**
PASM-Zn	1	1	900	11
Zn@PCFs	1	5	1500	12
NGO@Zn	0.5	0.25	2200	13
DES-Zn	3	2	800	14
$ZnSO_4$+Arg	1	10	300	15
ADC-gel	5	5	650	16
E-nHAP@Zn	10	5	400	17
MTSi-Hedp-Zn	1	1	1250	18
HEA-CFP	**1**	**0.5**	**3200**	**This work**
	10	**10**	**950**	**This work**

References

1. S. Boker, M. Neale, H. Maes, M. Wilde, M. Spiegel, T. Brick, J. Spies, R. Estabrook, S. Kenny, T. Bates, P. Mehta and J. Fox, *Psychometrika*, 2011, **76**, 306-317.

2. M. C. Neale, M. D. Hunter, J. N. Pritikin, M. Zahery, T. R. Brick, R. M. Kirkpatrick, R. Estabrook, T. C. Bates, H. H. Maes and S. M. Boker, *Psychometrika*, 2016, **81**, 535-

549.

3. T. Ozaki, *Phys. Rev. B*, 2003, **67**, 155108.

4. T. Ozaki and H. Kino, *Phys. Rev. B*, 2004, **69**, 195113.

5. P. E. Blöchl, *Phys. Rev. B*, 1994, **50**, 17953-17979.

6. J. P. Perdew, J. A. Chevary, S. H. Vosko, K. A. Jackson, M. R. Pederson, D. J. Singh and C. Fiolhais, *Phys. Rev. B*, 1992, **46**, 6671-6687.

7. J. P. Perdew and Y. Wang, *Phys. Rev. B*, 1992, **45**, 13244-13249.

8. S. Grimme, J. Antony, S. Ehrlich and H. Krieg, *The J. Chem. Phys.*, 2010, **132**, 154104.

9. Y. Tang, W. Chen, C. Li, L. Pan, X. Dai and D. Ma, *Appl. Surface Sci.*, 2015, **342**, 191-199.

10. L. Ma, J.-M. Zhang, K.-W. Xu and V. Ji, *Appl. Surface Sci.*, 2015, **343**, 121-127.

11. N. Wang, Z. Wu, Y. Long, D. Chen, C. Geng, X. Liu, D. Han, J. Zhang, Y. Tao and Q.-H. Yang, *J. Energy Chem.*, 2022, **73**, 277-284.

12. H. Ying, P. Huang, Z. Zhang, S. Zhang, Q. Han, Z. Zhang, J. Wang and W.-Q. Han, *Nano-Micro Lett.*, 2022, **14**, 180.

13. Y. Li, D. Zhao, J. Cheng, Y. Lei, Z. Zhang, W. Zhang and Q. Zhu, *Chem. Eng. J.*, 2023, **452**, 139264.

14. M. Kwon, J. Lee, S. Ko, G. Lim, S.-H. Yu, J. Hong and M. Lee, *Energy Environ. Sci.*, 2022, **15**, 2889-2899.

15. H. Lu, X. Zhang, M. Luo, K. Cao, Y. Lu, B. B. Xu, H. Pan, K. Tao and Y. Jiang, *Adv. Funct. Mater.*, 2021, **31**, 2103514.

16. Q. He, G. Fang, Z. Chang, Y. Zhang, S. Zhou, M. Zhou, S. Chai, Y. Zhong, G. Cao, S. Liang and A. Pan, *Nano-Micro Lett.*, 2022, **14**, 93.

17. K. Qi, W. Zhu, X. Zhang, M. Liu, H. Ao, X. Wu and Y. Zhu, *ACS Nano*, 2022, **16**, 9461-9471.

18. H. Yu, Y. Chen, H. Wang, X. Ni, W. Wei, X. Ji and L. Chen, *Nano Energy*, 2022, **99**, 107426.